Proceedings of the Institute of Acoustics

ON THE CHARACTERISTICS OF MODAL RADIATION FROM DUCTS ABOVE AND BELOW CUT-OFF

B. Baddour University of Southampton, Southampton, Hampshire, England
P. Joseph University of Southampton, Southampton, Hampshire, England
A. McAlpine University of Southampton, Southampton, Hampshire, England
R. Leung Defence Science Technology Laboratory, Fareham, Hampshire, England

INTRODUCTION

Ducts have a wide range of applications such as increasing the efficiency of engines, piping transport systems and exhaust stacks, all of which situate a noise source inside a finite length duct that radiate sound into an open space. Often one requires an indication of the sound field produced from such situations to quantify performance. Calculations are made simpler by making approximations, typically assuming the source is buried deep inside the duct. This allows the effect of cut-off modes to be neglected. This assumption may not be valid for several applications, especially ducted fans.

The distance between a noise source and a duct open end has been investigated by Howe,[1] who investigated the rotor blade tip vortex interaction noise for varying distances inside a duct. The approach Howe used is very different to that used here, as Howe did not break the source into its acoustic modes. The power radiated by cut-off modes was briefly investigated by Sandowaska[2] who investigated the power gain function of a duct mode slightly below cut-off, implying cut-off modes radiate to the far-field. In this paper we extend this work to form a model valid for all modes and using a Fourier approach we indicate the radiation efficiency of modes above and below cut-off.

A FOURIER APPROACH TO DUCT RADIATION

In this section we re-derive the classical radiation from a flanged duct formulation from Tyler and Sofrin,[3] using a Fourier approach. This allows us to separate radiating and non-radiating components of the velocity, and determine the components that radiate sound power. Consider an acoustic velocity distribution at the end of a rigid walled duct inside an infinite flange with radius a and surface area S. A source region on the flange with polar coordinates (r, θ, z) radiates with axial symmetry to a field point with spherical coordinates (R, ϕ, θ) as described by *Figure 1*.

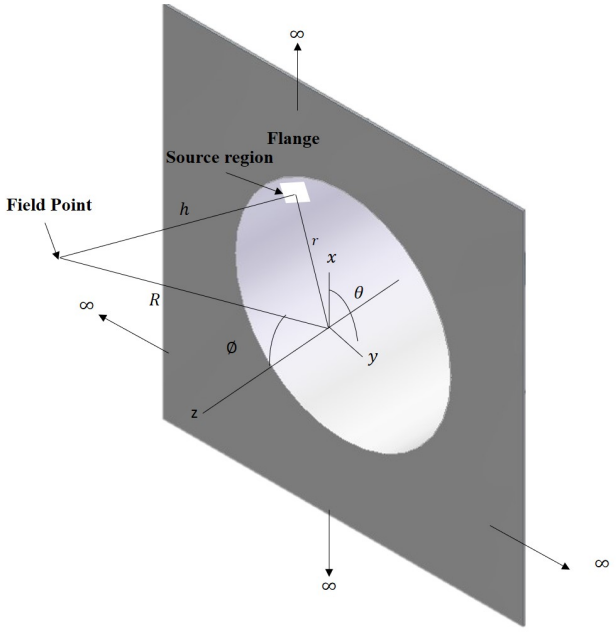

Figure 1: Semi-inifinite, hard walled flanged circular duct with associated coordinate system

Consider an axial velocity distribution $u_{mn}(r,\theta)$ over the duct opening at a single frequency, corresponding to a single mode of azimuthal order m and radial order n, with complex amplitude V_{mn}

$$u_{mn}(r,\theta) = V_{mn}\psi_{mn}(r)e^{jm\theta} \tag{1}$$

where $\psi_{mn}(r)$ is the normalized mode shape function, that ensures $\int_S |\psi_{mn}(r)|^2 dS = S$. The mode shape function for a hard-walled cylindrical duct is of the form

$$\psi_{mn}(r) = \frac{J_m(\kappa_{mn}r)}{N_{mn}} \qquad r \leq a \tag{2}$$

where J_m is the Bessel function of the first kind, κ_{mn} is the transverse wave number chosen to satisfy the hard walled boundary condition and N_{mn} is the normalization factor

$$N_{mn} = \sqrt{\left(1 - \frac{m^2}{\kappa_{mn}^2 a^2}\right)} J_m(\kappa_{mn}a). \tag{3}$$

In order to decompose the modal velocity distribution into radiating and non-radiating components the radial velocity distribution $u_{mn}(r)$ is now decomposed into wavenumber spectra $\hat{u}_{mn}(\kappa)$ by use of the Hankel transform

$$\hat{u}_{mn}(\kappa) = \int_0^\infty u_{mn}(r)J_m(\kappa r)rdr \tag{4}$$

The radial velocity distribution can be reconstructed from its spectral components by inverse Hankel transform

$$u_{mn}(r) = \int_0^\infty u_{mn}(\kappa) J_m(\kappa r) \kappa d\kappa. \tag{5}$$

Substituting (2) for the radial velocity into (4) and evaluating the integral gives

$$\hat{u}_{mn}(\kappa) = \frac{\kappa a}{\kappa_{mn}^2 - \kappa^2} \frac{J'_m(\kappa a)}{\sqrt{\left(1 - \frac{m^2}{\kappa_{mn}^2 a^2}\right)}}. \tag{6}$$

where the prime denotes differentiation with respect to its argument. The velocity distribution $u^r_{mn}(r, \theta)$ that radiates perfectly to the far-field - corresponding to $\kappa < k$ components where k is the excitation wavenumber for a given frequency ω and speed of sound c_0, defined as $\frac{\omega}{c_0}$ - is

$$u^r_{mn}(r) = \int_0^k \hat{u}_{mn}(\kappa) J_m(\kappa r) \kappa d\kappa, \tag{7}$$

The remaining velocity $u^{nr}_{mn}(r, \theta)$ components $k > \kappa$ therefore contribute only to the near-field

$$u^{nr}_{mn}(r) = \int_k^\infty \hat{u}_{mn}(\kappa) J_m(\kappa r) \kappa d\kappa. \tag{8}$$

It is also worthy of note that on the plane z = 0

$$u^r_{mn}(r) + u^{nr}_{mn}(r) = u_{mn}(r) \quad r \leq a \tag{9}$$

$$u^r_{mn}(r) + u^{nr}_{mn}(r) = 0 \qquad r > a \tag{10}$$

Where for $r > a$ the radiating and non-radiating components are equal and opposite.

Far-field radiation

We now consider the Rayleigh integral to determine the radiated acoustic pressure field $p_{mn}(R, \phi)$ of the form

$$p_{mn}(R, \phi) = \frac{j\rho_0 c_0 k}{2\pi} \int_S u_{mn}(r, \theta) \frac{e^{-jkh}}{h} dS(r, \theta) \tag{11}$$

where ρ_0 is the density, h is the distance between the source element and the field point

$$h = \sqrt{R^2 + r^2 - 2Rr \sin\phi \cos\theta}. \tag{12}$$

For large $R, h \approx R$ in the pressure amplitude and hence can be taken outside of the integral. The h inside the exponent can be written as $h \approx R - r \sin\theta \cos\phi$. Substituting these expressions for h, the Rayleigh integral becomes

$$p_{mn}(R, \phi) \approx \frac{jV_{mn}\rho_0 c_0 k e^{-jkR}}{2\pi R} \int_S u_{mn}(r) e^{jkr \sin\phi \cos\theta - jm\theta} dS(r, \theta). \tag{13}$$

Equations (1), (2) and (3) and the Hankel transform of $u^r_{mn}(r)$ from (7) can be combined and substituted into the Rayleigh integral,noting $dS = rdrd\theta$, to give

$$p_{mn}(R,\phi) \approx \frac{jV_{mn}\rho_0 c_0 k e^{-jkR}}{2\pi R} \int_0^{2\pi} \int_0^{\infty} \int_0^{k} \frac{\kappa^2 a}{\kappa_{mn}^2 - \kappa^2} \frac{J'_m(\kappa a)}{\sqrt{\left(1 - \frac{m^2}{\kappa_{mn}^2 a^2}\right)}} J_m(\kappa r)\kappa e^{jkr\sin\phi\cos\theta - jm\theta} r d\kappa dr d\theta. \tag{14}$$

The subsequent integral is evaluated using $\int_0^{2\pi} e^{jkr\sin\phi\cos\theta - jm\theta} = 2\pi j^m J_m(kr\sin\phi)$, from Rienstra and Hirschberg,[4] to give

$$p_{mn}(R,\phi) \approx \frac{j^{m+1}V_{mn}\rho_0 c_0 k e^{-jkR}}{R} \int_0^{\infty} \int_0^{k} \frac{\kappa^2 a}{\kappa_{mn}^2 - \kappa^2} \frac{J'_m(\kappa a)}{\sqrt{\left(1 - \frac{m^2}{\kappa_{mn}^2 a^2}\right)}} J_m(\kappa r) J_m(kr\sin\phi) r d\kappa dr d\theta. \tag{15}$$

The radial integral is evaluated using the identity $\int_0^{\infty} J_m(\kappa r) J_m(kr\sin\phi) r dr = \frac{\delta(\kappa - k\sin\phi)}{\kappa}$, from Rienstra and Hirschberg,[5] to give

$$p_{mn}(R,\phi,\kappa) \approx \frac{j^{m+1}V_{mn}\rho_0 c_0 k e^{-jkR}}{R} \int_0^{k} \frac{\kappa a}{\kappa_{mn}^2 - \kappa^2} \frac{J'_m(\kappa a)}{\sqrt{\left(1 - \frac{m^2}{\kappa_{mn}^2 a^2}\right)}} \delta(\kappa - k\sin\phi) d\kappa, \tag{16}$$

Noting the sifting property of the delta function suggests that each velocity component κ only radiates to a single far field radiation angle ϕ, given by

$$\phi = \sin^{-1}\frac{\kappa}{k}. \tag{17}$$

The far field pressure is identical to the classical result derived by Tyler and Sofrin[3] which is

$$p_{mn}(R,\phi) \approx \frac{j^{m+1}V_{mn}\rho_0 c_0 e^{-jkR}}{\frac{R}{a}} D_{mn}(\phi). \tag{18}$$

Where the directivity factor D_{mn} is

$$D_{mn}(\phi) = \frac{\sin\phi J'_m(ka\sin\phi)}{(\frac{\kappa_{mn}^2}{k^2} - \sin^2\phi)\sqrt{\left(1 - \frac{m^2}{\kappa_{mn}^2 a^2}\right)}}. \tag{19}$$

Modal radiation about cut-off

In order to determine the relative contribution of the axial velocity distribution $u_{mn}(r)e^{-jm\theta}$ to the far-field and near-field region a plot of the wavenumber velocity spectrum for a typical mode $m = 9, n = 6$ excited below cut-off plotted against $\frac{\kappa}{\kappa_{mn}}$, and $m = 12, n = 10$ excited above cut-off is shown in *Figure 2*. Also shown in the Figure is a vertical line that indicates the excitation wavenumber, which determines the transition between the radiating ($k < \kappa$) and non-radiating ($\kappa > k$) components.

To quantify how cut-off a mode is, we define the cut-off ratio ζ as

$$\zeta = \frac{k}{\kappa_{mn}} \tag{20}$$

where $1 < \zeta < \infty$ indicates a cut-on mode and $0 < \zeta < 1$ indicates a cut-off mode.

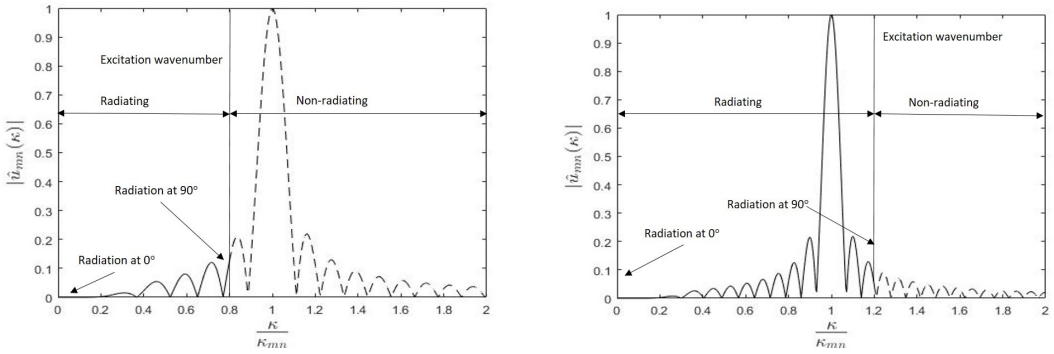

Figure 2: Velocity spectrum for mode m = 9, n = 6, ζ = 0.8 (left) and m = 12, n = 10, ζ = 1.2 (right)

The analysis above has demonstrated a direct relationship between the far-field directivity $D_{mn}(\phi)$ and the modal velocity wavenumber spectrum $\hat{u}_{mn}(\kappa)$ where $\kappa = k \sin \phi$. The velocity spectrum at $\kappa = k$ therefore gives the radiation at 90° to the duct axis and $\kappa = 0$ gives the radaition at 0°. The velocity spectrum between 0° and 90° will then directly map to the directivity, matching turning points to lobes. We now excite the mode $m = 9, n = 6$ just below cut-off at $\zeta = 0.95$ and just above cut-off at $\zeta = 1.05$ and compute the radiating and non-radiating $\psi(r)e^{-jm\theta}$, shown in *Figure 3*.

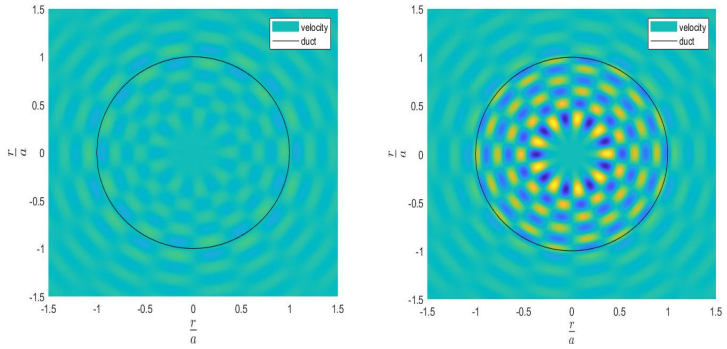

(a) mode (9,6) ζ = 0.95, radiating (left) and non-radiating velocity components (right)

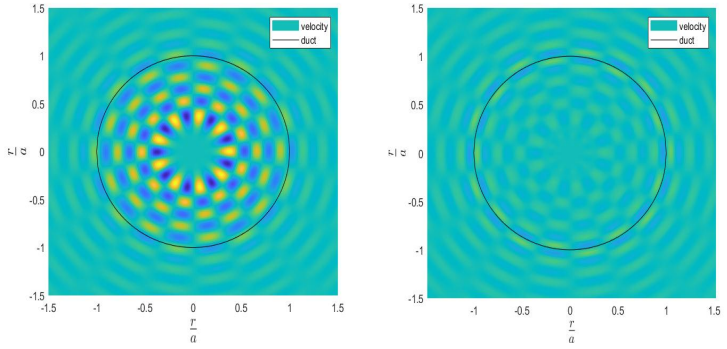

(b) mode (9,6) ζ = 1.05, radiating (left) and non-radiating velocity components (right)

Figure 3: Radiating and non-radiating velocity distributions above and below cut-off

Figure 3 shows that for $\zeta = 0.95$, most of the velocity at the end of the duct does not propagate,

however, the figure shows that a small amount of velocity propagates to the far-field for excitation below cut-off. The figure also shows that for $\zeta = 1.05$, most of the velocity propagates to the far-field but there is a small amount that does not radiate. In the high frequency limit all velocity radiates to the far-field and in the low frequency limit no velocity radiates.

Directivity above and below cut off

We have demonstrated that below cut-off some components of the modal velocity distribution radiate to the far field. Using (19) we plot far field directivity functions for excitation just above and just below cut-off - which has an identical pattern to $\hat{u}(\kappa)$. The plots shown are scaled so that the pressure at the major lobe is 100 dB for the plot that is excited at the highest frequency. *Figure 4* shows the directivity of the mode $m = 9, n = 6$ for $\zeta = 0.3, 0.9, 1.1$ and 1.2.

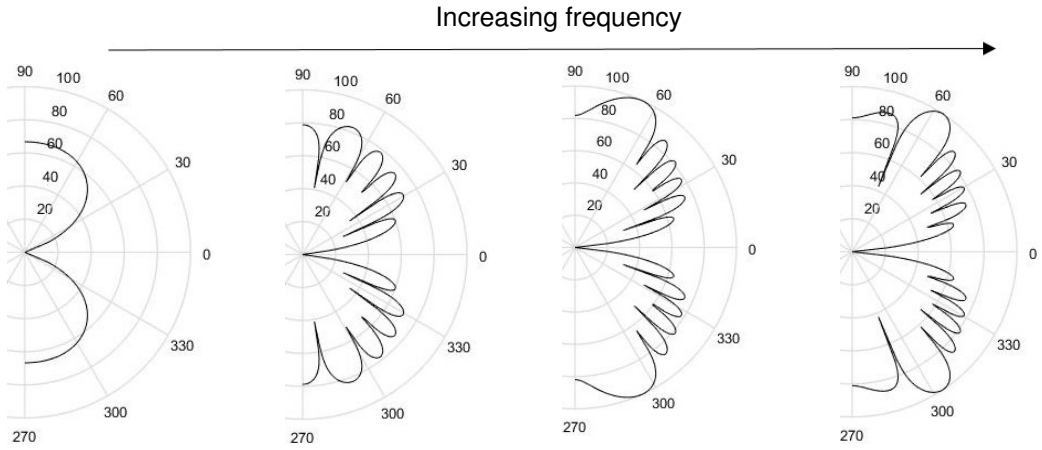

(a) ζ = 0.3 (cut-off) **(b) ζ = 0.9 (near cut-on)** **(c) ζ = 1.1 (cut-on)** **(d) ζ = 1.2 (cut-on)**

Figure 4: Directivity above and below cut-off of the mode m = 9, n = 6

An important observation from *Figure 4* is the location of the major lobe which can be identified into 3 regions; in the cut-on region the major lobe approaches the sideline directions, in the near cut-on region, the major lobe will vary between 90° and near 90° somewhere in the sideline directions. This behavior is determined by the spectrum in *Figure 2* as the major lobe will be located at the highest peak of $\hat{u}_{mn}(\kappa)$ below k which is not necessarily at 90°. This variation of the major lobe position occurs until the last turning point of $\hat{u}_{mn}(\kappa)$ is reached with respect to decreasing wavenumber, and then the directivity will have identical shape for all frequencies with the major lobe located at 90°. The wavenumber k_{cut} that transitions from the near cut-on to the cut-off region occurs at the 1st turning point of $\hat{u}(\kappa)$

$$\left.\frac{d\hat{u}_{mn}(\kappa)}{d\kappa}\right|_{min} = 0.$$

Exciting the mode at or below $\kappa = k_{cut}$ there is no dominating lobe in the directivity. It can be seen from (4) that the turning points are supplied by $J'_m(\kappa a)$, where the turning points of $J'_m(\kappa a)$ match well with $u_{mn}(\kappa)$, therefore the transition between the near cut-on and cut-off region can be determined approximately by the minimum wavenumber that satisfies $J''_m(k_{cut}a) = 0$. Which is always below the modal transverse wavenumber of the first radial mode, hence

$$\Omega_{cut} \leq c_0 \kappa_{m,1}.$$

Radiation efficiency

Morfey[6] calculated the modal radiation efficiency τ_{mn}, for modes above and below cut-off to show the maximum radiation efficiency is around cut-off. To calculate the modal power we use (18) and (17) to infer the far-field pressure distribution in terms of the incident velocity wave number spectral components κ, which is required for the proceeding numerical analysis.

$$p_{mn}(\kappa) \approx \frac{j^{m+1} V_{mn} \rho_0 c_0 k e^{-jkR}}{R} \frac{J'_m(\kappa a)\kappa a}{(\kappa_{mn}^2 - \kappa^2)\sqrt{\left(1 - \frac{m^2}{\kappa_{mn}^2 a^2}\right)}}. \tag{21}$$

To calculate the power, we integrate the radial intensity across a hemisphere enclosing the duct opening of radius R, $W_{mn} = \frac{\pi}{\rho_0 c_0} R^2 \int_0^{\frac{\pi}{2}} |p_{mn}(R,\phi)|^2 \sin\phi \, d\phi$ and use the substitution $\kappa = k \sin\phi$ and $d\kappa = \sqrt{k^2 - \kappa^2} d\phi$ to derive

$$W_{mn} = \frac{\pi}{\rho_0 c_0} R^2 \int_{\kappa=0}^{\kappa=k-\epsilon} |p_{mn}(\kappa)|^2 \sqrt{\frac{\kappa^2}{k^4 - (k\kappa)^2}} d\kappa. \tag{22}$$

where ϵ is a very small value to avoid evaluation at $\kappa = k$, where the integrand becomes singular, the integration is not sensitive to the size of ϵ. The modal radiation efficiency τ_{mn} is calculated as

$$\tau_{mn} = \frac{W_{mn}}{\frac{1}{2}|V_{mn}|^2 \pi a^2 \rho_0 c_0}. \tag{23}$$

Substituting (21) and (22) into (23) gives

$$\tau_{mn} = \frac{2}{\left(1 - \frac{m^2}{\kappa_{mn}^2 a^2}\right)} \int_0^{k-\epsilon} \left(\frac{J'_m(\kappa a)}{(1 - \frac{\kappa_{mn}^2}{\kappa^2})} \right)^2 \frac{1}{\kappa} \sqrt{\frac{1}{1 - \left(\frac{\kappa}{k}\right)^2}} d\kappa \tag{24}$$

Figure 5 shows the radiation efficiency of modes $m = 1, 2, 3, 4$ for $n = 1$ and $n = 2$, note $m = 0, n = 1$ is always cut-on so was avoided.

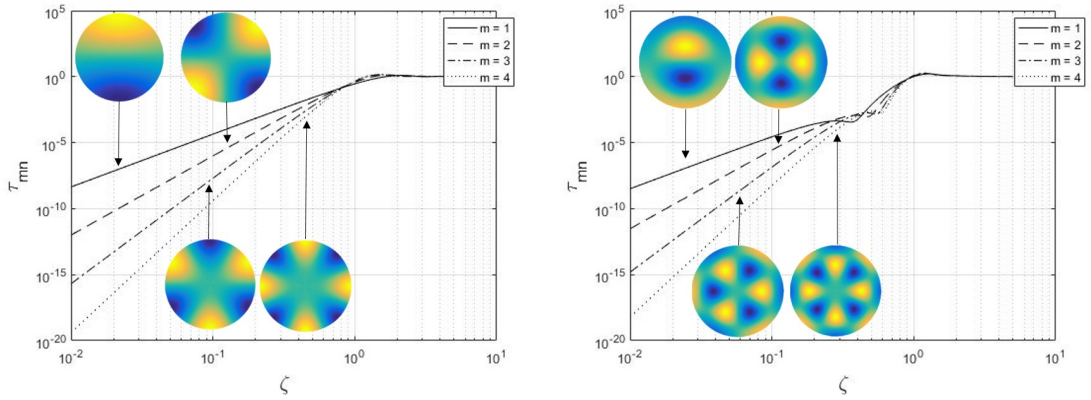

Figure 5: Radiation efficiency of the modes m = 1, 2, 3, 4 for n = 1 (left) and n = 2 (right), shown with the associated mode shapes

Figure 5 shows that the radiation efficiency of all modes have a resonance peak around cut-off of approximately 1. The figure shows that increasing azimuth increases the asymptotic low

frequency fall off of τ_{mn}. Morfey[6] showed that $\tau_{mn} \propto (ka)^{2m+2}$ in the low frequency limit, which agrees with the Figure. It is also worthy of note that mode $m = 1, n = 1$ acts as a dipole which has $\tau_{mn} \propto (ka)^4$, a classical result. The Figure shows that modes of the same radial order n have the same low frequency asymptotic fall off. To investigate this independence of n, *Figure 6* shows the radiated components of the mode $m = 9, n = 6$ and $m = 12, n = 10$ for $\zeta = 0.50$ and a plot of the modulus of the radial velocity against radial distance from the center of the duct of the mode $m = 9, n = 6$ for $\zeta = 1.00, 0.10$ and 0.01, calculated using (7).

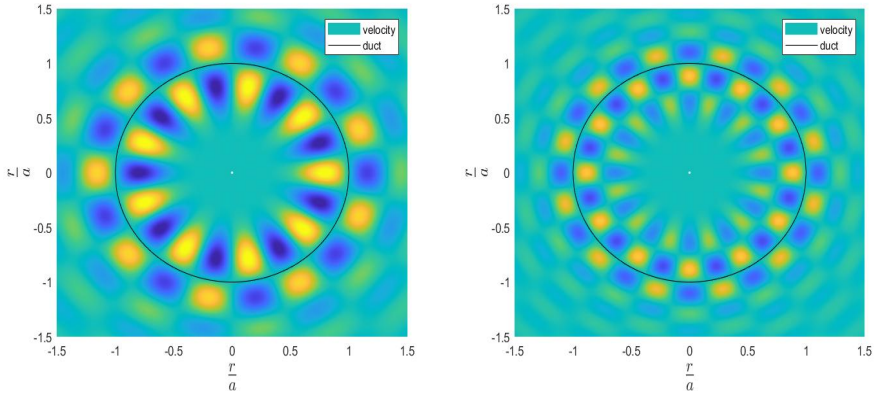

Figure 6: Radiating velocity of the mode (9,6 left) and (12,10 right) for ζ = 0.50

Figure 6 shows the radiation is localized towards the edge of the duct, showing the low frequency asymptotic behavior of modes is identical to classic edge effect radiation. This gives explanation to why the efficiency of the modes is independent of n, as the number of nodal circles do not affect the radiation at the circumference of the duct, which are the dominating radiated components of the low frequency asymptotic behavior. From the radial velocity plot in the Figure it can be seen that the location of the maximum velocity moves further outside the duct with decreasing frequency. At cut-off the maximum radiated velocity is located at the duct wall, and the maximum velocity within the duct is always located at the wall showing the edge effects.

The relationship between τ_{mn} and ka is investigated mathematically by representing the Bessel function in terms of an infinite series defined as

$$J_m(\kappa a) \rightarrow \sum_{v=0}^{\infty} \frac{-1^v(\kappa a)^{(m+2v)}}{2^{(m+2v)}v!(m+v)!}. \tag{25}$$

Taking the differential, squaring and substituting into (24) gives

$$\tau_{mn} = \frac{2B_{mn}}{\left(1 - \frac{m^2}{\kappa_{mn}^2 a^2}\right)} \int_0^{k-\epsilon} \sum_{v=0}^{\infty} \sum_{v'=0}^{\infty} (\kappa a)^{(2m+2v+2v'-2)} \left[\frac{1}{(1 - \frac{\kappa_{mn}^2}{\kappa^2})^2}\right] \frac{1}{\kappa} \sqrt{\frac{1}{1 - \left(\frac{\kappa}{k}\right)^2}} d\kappa \tag{26}$$

where for brevity the constant B_{mn} is defined

$$B_{mn} = \sum_{v=0}^{\infty} \sum_{v'=0}^{\infty} \frac{-1^{(v+v')}(m+2v)(m+2v')}{2^{(2m+2v+2v')}v!v'!(m+v)!(m+v')!} \tag{27}$$

The radiation efficiency has it's most interesting properties for low frequencies at low κa, acknowledging κa is bounded by 0 and ka. For small κa the approximation $\kappa a << \kappa_{mn} a$ can be made, multiplying numerator and denominator by $(\kappa a)^2$ for the fraction in the square bracket

allows $(\kappa_{mn}a)^4$ to be taken out of the integrand, note that to absorb $\frac{1}{\kappa}$ into $(\kappa a)^{2m+1}$ requires multiplication by a, giving

$$\tau_{mn} \approx \frac{2aB_{mn}}{(\kappa_{mn}a)^4\left(1-\frac{m^2}{\kappa_{mn}^2a^2}\right)} \int_0^{k-\epsilon} \sum_{v=0}^{\infty}\sum_{v'=0}^{\infty} (\kappa a)^{(2m+2v+2v'+1)} \sqrt{\frac{1}{1-\left(\frac{\kappa}{k}\right)^2}}\, d\kappa \tag{28}$$

using the substitution $b = m + v + v'$ and $s = \frac{\kappa}{k}$, where $d\kappa = kds$ gives

$$\tau_{mn} \approx \frac{2B_{mn}}{(\kappa_{mn}a)^4\left(1-\frac{m^2}{\kappa_{mn}^2a^2}\right)} \sum_{v=0}^{\infty}\sum_{v'=0}^{\infty} (ka)^{(2b+2)} \int_0^1 s^{(2b+1)} \sqrt{\frac{1}{1-s^2}}\, ds \tag{29}$$

From Gradshteyn and Ryzhik[7] $\int_0^1 s^{(2b+1)} \frac{1}{\sqrt{1-s^2}} ds = \frac{(2b)!!}{(2b+1)!!}$, where $b!! = b \times (b-2) \times (b-4)...$ and the last multiplier is 1 for odd or 2 for even b, solving the integral gives

$$\tau_{mn} \approx \frac{2B_{mn}}{(\kappa_{mn}a)^4\left(1-\frac{m^2}{\kappa_{mn}^2a^2}\right)} \sum_{v=0}^{\infty}\sum_{v'=0}^{\infty} (ka)^{(2(m+v+v')+2)} \frac{(2(m+v+v'))!!}{(2(m+v+v')+1)!!} \tag{30}$$

The number of terms used is investigated to form a more practical formulation. The special case of only considering the first term (zeroth term) is of the form

$$\tau_{mn} \approx (ka)^{2m+2} \frac{(2m)!!}{\kappa_{mn}^4 a^4 (1-\frac{m^2}{\kappa_{mn}^2a^2}) 2^{2m-1}(m-1)!^2(2m+1)!!}. \tag{31}$$

It can be seen from (31) that the proportionality relationship $\tau_{mn} \propto (ka)^{2m+2}$ derived by Morfey[6] is highlighted . Increasing m sharply decreases the efficiency. Clearly therefore the cut-off modes are only important for low order azimuthal modes. The weak dependence on n is shown in the equation by κ_{mn} in the denominator which slowly increases with n, but n has considerably less influence than m. Another case worthy of note is considering the sum to n terms (considering the zeroth to the $n-1$ term). *Figure 7* shows a comparison between the numerical expression for τ_{mn} from (24), the approximate expression for τ_{mn} from (30), plotted against ζ for the modes $m = 1$ $n = 1, 2$ and 10 considering one and n terms.

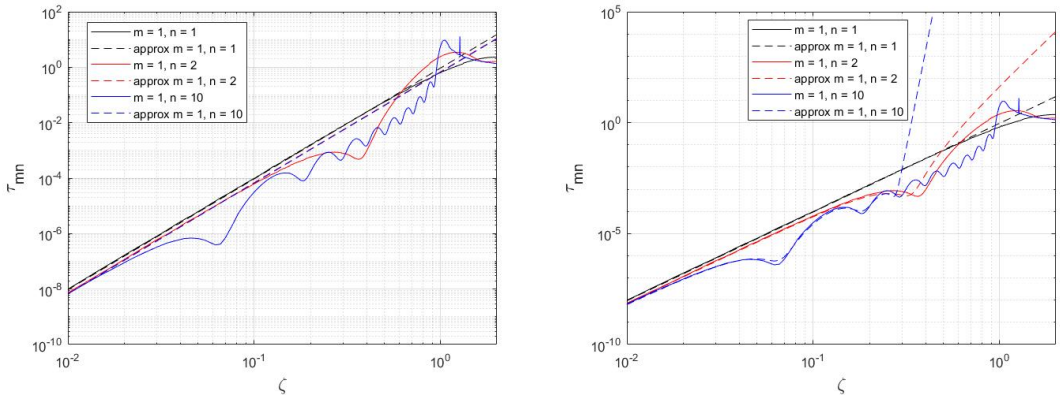

Figure 7: Comparison between exact and approximate expression for τ_{mn} for the modes m = 1, n = 1, 2 and 10 considering one (left) and n terms (right) in (30)

Figure 7 shows that the exact and analytic equations converge for small ζ. The Figure shows that the larger n result in more oscillations before the solution settles to the first term approximation,

the number of oscillation is proportional to n, the frequency of the turning points are located at the cut-off frequencies for modes of lower radial order, hence why the $n = 10$ case has 10 turning points corresponding to the cut-off ratios of $n = 9, 8$ etc. The very small dependence on n is also demonstrated at very low frequency, although near cut-off the efficiency is dependent on m and n. The first term is shown to be dominant at low frequency and for the $n = 1$ case.

Conclusion

In this paper we have shown that cut-off modes potentially radiate to the far-field efficiently, mostly affecting the sideline directions. We have derived an expression that allows the behavior of a single mode to be understood - using a Fourier approach to decompose the velocity into radiating and non-radiating components. We have presented 3 regions of directivity that indicate the location of the major lobe - which near cut-off is around 90 °.

Decomposing the waves allows us to explain mathematically and physically a result published by Morfey,[6] that the low frequency asymptotic behavior of the efficiency behaves as $\tau_{mn} \propto (ka)^{2m+2}$, implying the most important cut-off modes are those of lowest azimuthal order. An approximate expression for τ_{mn} has been derived which (for $\zeta < 1$) matches very well for $n = 1$, we have shown that the approximation can encompass $n > 1$ modes by considering a summation to n terms in the expression. This work is most applicable when the source is located near the open end of the duct, which is often the case for marine ducted fans.

Acknowledgments

Funding for this work was gratefully accepted by the Engineering and Physical Sciences research council and the Defense Science Technology Laboratory.

References

[1] MS Howe. Installation effects on the production of blade-vortex interaction noise by a ducted rotor. *Journal of sound and vibration*, 156(1):61–78, 1992.

[2] Anna Snakowska and Jerzy Jurkiewicz. Efficiency of energy radiation from an unflanged cylindrical duct in case of multimode excitation. *Acta Acustica united with Acustica*, 96:416–424, 2010.

[3] John M Tyler and Thomas G Sofrin. Axial flow compressor noise studies. Technical report, SAE, 1962.

[4] Sjoerd W Rienstra and Avraham Hirschberg. An introduction to acoustics. *Eindhoven University of Technology*, 18:252, 2004.

[5] Sjoerd W Rienstra and Avraham Hirschberg. An introduction to acoustics. *Eindhoven University of Technology*, 18:253, 2004.

[6] CL Morfey. A note on the radiation efficiency of acoustic duct modes. *Journal of Sound and Vibration*, 9(3):367–372, 1969.

[7] IS Gradshteyn, IM Ryzik, and Alan Jeffrey. *Table of Integrals, Series, and Products*. Section 3.248, p 294, 1980.